

MORPHOLOGICAL, MECHANICAL, ORGANIC VAPOUR PERMEATION PROPERTIES AND BIODEGRADABILITY OF POLY(ETHYLENE-CO-VINYL ACETATE)/WASTE PISTACHIO SHELL-DERIVED CELLULOSE COMPOSITE MEMBRANES

SHANA JEBIN VALIYA PEEDIYAKKAL,* RAJESH CHERUMADATHIL** and FASEENA NAMBIDUMANNIL*

*Department of Chemistry, MES Mampad College (Autonomous),
Affiliated to University of Calicut, Kerala 676542, India

**Department of Chemistry, MES Kalladi College, Mannarkkad, Affiliated to University of Calicut, Kerala 678583, India

✉ Corresponding author: Faseena Nambidumannil, faseena@mesmampadcollege.edu.in

Received August 8, 2023

Cellulose fibers have attracted interest as a suitable candidate for manufacturing composites. In the present work, cellulose derived from waste pistachio shell was used to prepare composite membranes with poly(ethylene-co-vinyl acetate) (EVA) via solution casting, and their morphological, mechanical, organic vapour permeation characteristics and biodegradability were evaluated. Scanning electron micrographs showed that the voids in the EVA polymer were filled effectively by cellulose fibers. The mechanical testing of the composites revealed an improvement in Young's modulus with the increase in cellulose loading. The permeation of polar and non-polar solvents through the membranes was studied and explained by molar size, molecular mass and polarity of the solvents. Nielson's permeability equation as modified by Baradwaj was used to analyse the relative permeability of the membranes. Soil burial degradation experiments of the composite membranes showed a decrease in weight and tensile strength, revealing the biodegradability of the membranes.

Keywords: ethyl vinyl acetate-cellulose membranes, pistachio shell, vapour permeation, biodegradability

INTRODUCTION

Increased concerns over the environmental issues caused by synthetic fiber based polymer composites have led scientists to search for renewable eco-friendly materials for a sustainable world. Natural fibers, such as kenaf, hump, jute, sisal, coconut, banana *etc.*, were identified as suitable materials having properties that match those of synthetic fibers. Moreover, the lower weight, high strength, good resistance to corrosion and fatigue, lower cost and wide availability of cellulose fibers have promoted their use in place of synthetic fibers to produce cellulose fiber polymer composites.¹ Such composites have found applications in aerospace and building industries, in automotive components and packaging applications to name just a few.²

Packaging materials for food and medicine require superior barrier resistance against oxygen, moisture, carbon dioxide and organic vapours. Commonly used packaging materials include synthetic polymers, such as ethyl vinyl alcohol, poly(ethylene terephthalate), polyolefin, polyamide *etc.*, due to their advantageous mechanical, thermal and barrier properties.³ The barrier properties of packaging materials can be enhanced through strategies, such as blending or coating of substances with high barrier materials, developing filler-polymer systems and the use of multi-layered membranes containing high barrier materials.⁴

The addition of fillers into the polymer matrix accompanies the inclusion of voids by the filler particle and thus inhibits permeation of various substances through the composite membranes.

The homogenous dispersion of impermeable particles acts as an obstacle for penetrating molecules. The penetrant must go around these impermeable flakes, creating a tortuous path for the molecules. This tortuosity depends on various factors related to the filler, such as size, shape, orientation and aspect ratio.⁵ When fiber size decreases, the dispersion of the filler in the polymer becomes more effective, which inhibits agglomeration and fills up the voids of the polymer successfully, thus makes the polymer membrane impermeable to gases and vapours. The effect of filler shape on the barrier properties of polymer/non-porous particles nanocomposites was studied and it was found that the relative permeability is reduced significantly with layered nanoparticles.⁶ The filler particles can take perpendicular, parallel and random orientation in a polymer matrix, but an optimal decrease in permeability is obtained when the alignment of the filler surface is perpendicular to the direction of gas/vapour permeation.⁷ Nanocomposites of hydrogenated acrylonitrile butadiene rubber with montmorillonites were prepared and fluorohectorite, both modified with octadecylamine, and it was found that fluorohectorite with high aspect ratio causes a decrease in oxygen permeability to a greater extent.⁸ We cannot attribute the tortuosity effect to a single factor, modifications in tortuosity occur due to on each and every factor described above, as well as the molecular mass of the polymer, the free volume, voids, crystallinity, the creation of interphase *etc.*, thereby, permeability also changes.

Poly(ethylene co-vinyl acetate) – EVA – is an advanced material having fascinating applications, such as packaging, biomedical devices, toys, footwear, cable insulation and others.⁹ EVA has been studied by researchers due to its gas separation performance, as well as gas barrier properties.¹⁰⁻¹² The amorphous filler increases the gas permeability performance of EVA composite membranes, while more crystalline filler increases their barrier performance. EVA/clay nanocomposite membranes were prepared and studied in terms of the permeation of oxygen and nitrogen gases through the membranes.¹³ The study confirmed that 3% clay loading exhibited better homogeneous dispersion and lower oxygen and nitrogen gas permeability. The authors also found that agglomeration increased at higher clay loading. A comparison of experimental and

theoretical permeability using the Baradwaj model confirmed agreeability with the model at lower percentage of clay loading. The oxygen barrier performance of EVA/calcium phosphate nanocomposites was studied and it was found that the tortuous path produced by the nanosized filler particles caused a decrease in oxygen permeability.¹⁴ The performance of gas separation attributed to EVA/nanosilica composite membranes was investigated and the results showed an increased permeability of all gases and selectivity of CO₂/CH₄ and CO₂/N₂ gases with an increase in silica content.¹⁰

Cellulose is an abundant biopolymer, which is a major component of natural fibers. Cellulosic materials, such as nanofibrillated cellulose, nanocrystalline cellulose, microcrystalline cellulose, bacterial cellulose *etc.*, are used to prepare high barrier performance composite membranes.¹⁵ Biodegradable membranes from tapioca starch as matrix and microcrystalline cellulose as filler were developed and their oxygen and water vapour permeation performance were studied.¹⁶ The researchers found that the incorporation of 3% of microcrystalline cellulose into starch results in greater barrier performance. The reactive extrusion process to fabricate polylactic acid (PLA)/nanocrystalline cellulose (CNC) membranes for the applications in food packaging was used.¹⁷ The addition of acid derived CNCs (H₂SO₄ derived CNCs and HCl derived CNCs) to the PLA matrix showed a drop in oxygen permeation values of the membrane. It was about 20% for H₂SO₄ derived CNCs and ~40% for HCl derived CNCs. The decrease in oxygen permeation of H₂SO₄ derived CNCs/PLA membrane is due to the more tortuous pathway created by the filler with a higher aspect ratio compared to that of HCl derived CNCs. The study also showed a reduction in water vapour permeability by 42% for both CNC membranes.¹⁷ Apart from the studies mentioned above, various research endeavours have underscored the efficacy of EVA¹⁸⁻²⁰ and cellulose²¹⁻²³ as formidable contributors to barrier performance. Notably, semicrystalline EVA exhibits enhanced permeation characteristics when reinforced with impermeable cellulose fibers, and natural fibers are recognized as optimal sources of cellulose.

Pistachio shells are one of the most abundantly available agricultural wastes, and it is often discarded or fed to animals or incinerated. Pistachio shells are a by-product of the pistachio nut industry, and they can offer a multitude of

benefits – they can be utilized for mulch, compost, crafts, fuel, and animal padding. Extracts from pistachio shells hold promise considering their antioxidant, anti-inflammatory and other medicinal properties.²⁴ After appropriate processing, they can be incorporated into animal feed, providing a source of nutrients.²⁵ Additionally, these shells serve as a valuable source of cellulose. The composition of pistachio shells allows the biosynthetic development of various products, such as biofuels, bioplastics or other biochemicals.²⁶ The porous nature of pistachio shells also enables the filtration and adsorption of pollutants during waste water treatment.²⁷ In the current study, pistachio shells serve as a cellulose source for the fabrication of composite membranes with EVA.

Numerous studies discuss the viability of incorporating pistachio shells as fillers in polymer composites. Nayek *et al.* observed that the introduction of pistachio shell flakes resulted in enhanced flexural and impact properties in polyester composites, however, it led to a reduction in tensile properties.²⁸ Karağaç *et al.* found that incorporating ground pistachio shell as a filler in natural rubber/styrene butadiene compounds improved abrasion resistance, but resulted in lower tensile strength.²⁹ Thiagarajan *et al.* demonstrated that the inclusion of pistachio shell particles enhanced the tensile and flexural strength of glass fiber/epoxy polymer composites.³⁰ Beyond mechanical improvements, pistachio shells serve as valuable resources of cellulose, promoting sustainability, minimizing environmental impact, supporting economic efficiency, contributing to a circular economy by closing the loop on waste streams.

Interestingly, while the utilization of waste pistachio shells for cellulose production is recognized, there remains an unexplored avenue in employing this cellulose to enhance the barrier properties of ethylene-vinyl acetate (EVA) membranes. The current study intends to fill this gap by preparing composite membranes of EVA and cellulose derived from waste pistachio shells. The research seeks to explore the reinforcing capacity of this filler, to investigate the characteristics of the composite membranes in organic vapour permeation and their biodegradability. This research endeavours to contribute to the broader understanding of sustainable materials and their potential applications in membrane technology.

EXPERIMENTAL

Materials

Approximately 2 kg of pistachio shells, generated after the consumption of nuts, were procured from various bakery shops. Poly(ethylene-co-vinyl acetate (EVA-28) was purchased from N. Shashikant & Co. Speciality Chemicals, Mumbai, India. The reagents used for the pretreatments of pistachio shells were of analytical grade. Tetrahydrofuran (THF) was supplied by Qualigens, Thermofisher Scientific India Pvt. Ltd., Mumbai, India. The solvents used in the vapour permeation studies were of analytical purity.

Extraction of cellulose fibers from pistachio shells

The filler used for EVA matrix composite membrane production was cellulose derived from pistachio shells. Collected pistachio shells were washed thoroughly and dried well. The dried pistachio shells were ground well to get fine powder and sieved through 250 μm mesh. The pistachio shell powder was subjected to treatment with 1M sodium hydroxide at 80 °C for 4 hours to remove hemicelluloses and lignin. The product obtained was washed many times with distilled water and well dried. The alkali treated pistachio shell powder was then bleached using 2% sodium hypochlorite and 5% acetic acid at 80 °C for 5 hours, washed well and dried until constant weight. The total removal of lignin and hemicelluloses was ensured by repeating the process five times.

Fabrication of EVA/cellulose composite membranes

EVA28/cellulose composite membranes were fabricated using the solution casting technique. Initially, 6 g of EVA was weighed and then dissolved in 80 mL THF under heating at 50 °C for a duration of 3 hours. Subsequently, varying amounts of cellulose (0, 0.15 g, 0.3 g, 0.45 g, and 0.6 g representing different weight percentages) were dispersed in the same solvent. This cellulose dispersion was then combined with the EVA and THF solution and treated once again at 50 °C for 10 minutes. The resulting solution was cast in a glass Petri dish of 16 cm diameter, and the solvent was allowed to evaporate at room temperature in a fume hood. Five types of composite membranes were prepared with varying weights of cellulose, namely 0, 0.15 g, 0.3 g, 0.45 g, and 0.6 g, corresponding to 0, 2.5, 5, 7.5, and 10 weight percentages, respectively. The formulations of these five types of composites are given in Table 1. The fabricated membranes had 0.3 ± 0.03 mm thickness.

Vapour permeability of membranes

Vapour permeability measurements were done using specially designed vials. A particular amount of solvent was introduced in small vials and the composite membrane was placed tightly on the mouth of the vials. The weight loss was monitored at 10 minutes intervals over a span of two hours. The

selected solvents for permeation included: dichloromethane, chloroform, carbon tetra chloride (polar solvents/chlorosolvents), as well as benzene, toluene and xylene (non-polar solvents/BTX solvents). The membrane area in the permeation study was 1.76 cm².

The investigation focused on the permeation of both polar and non-polar solvents through the prepared

composite membranes. The permeation coefficients and relative permeability of polymer composite membranes were also determined to get a quantitative measure of permeation and gain insights into the underlying transport mechanisms. The equations employed for calculating permeation coefficients and relative permeability are provided below.

Table 1
Composition of membranes

Sample code	EVA28 (g)	Cellulose (wt%)
EVAC0	6	0
EVAC1	6	2.5
EVAC2	6	5
EVAC3	6	7.5
EVAC4	6	10

The permeation coefficients of composite membranes were calculated using the equation:³¹

$$P = \frac{QL}{\Delta PAt} \quad (1)$$

where the molar quantity of solvent permeated is represented by Q , L indicates the thickness of the membrane, ΔP is the difference in partial pressure, A is the membrane area through which the solvent molecules permeated and t is the time taken by the vapour to permeate.

Relative permeability of the EVA/cellulose composites was calculated theoretically and determined experimentally, and the values were compared. It was calculated using Nielson's permeability equation modified by Baradwaj:³²

$$\frac{P_c}{P_m} = \frac{1-\phi}{1+\alpha\phi^{\frac{2}{3}}(S+\frac{1}{2})} \quad (2)$$

where P_c and P_m are the permeation coefficient of the EVA/cellulose composite and the permeation coefficient of the pure EVA membrane, respectively, ϕ and α indicate the volume fraction and the aspect ratio of the filler in the EVA matrix. S is the order parameter indicating the orientation of the filler in the matrix ($S = \frac{1}{2}(3\cos^2\theta - 1)$). The aspect ratio (α) is given

by the equation $\frac{l}{2w}$ where l and w are the length and

width of the cellulose fiber. S can have values of 1, 0 or $-\frac{1}{2}$ corresponding to parallel, random and perpendicular orientation of the filler in the matrix. Here, parallel and random orientations of the filler in the matrix were considered.

Soil burial test

Biodegradation studies of EVA/cellulose composite membranes were carried out by the soil burial test. The soil burial test was done with the primary objective of examining the influence of cellulose on the non-

biodegradable EVA polymer. The samples of EVA pure polymer membrane (EVAC0), EVA/cellulose 5% composite membrane (EVAC2) and EVA/cellulose 7.5% composite membrane (EVAC3) were selected for studies. Rectangular specimens for tensile strength analysis and circular discs for weight loss measurements were cut from the samples, buried under the soil for two months at a depth of 20 cm, and allowed to biodegrade. After two months, the samples were taken out, washed with distilled water thoroughly to remove dirt and dried until constant weight. The weight loss of the samples was measured using the equation:

$$\text{Percentage weight loss} = \frac{w_i - w_f}{w_i} \times 100 \quad (3)$$

where w_i and w_f are the initial and final weight of the samples buried in the soil.³³ The tensile strength of the samples was also evaluated before and after the soil burial test and loss in tensile strength was also calculated.

Fourier transform infrared spectral analysis

An FTIR spectrophotometer (IR Affinity 1S-Shimadzu) was used to record the FTIR spectra of composite membranes, pistachio shell powder and cellulose in the range of 600 and 4000 cm⁻¹, with an average of 45 scans and resolution of 4 cm⁻¹.

Scanning electron microscopic analysis

A scanning electron microscope (Model ZEISS Gemini SEM 300) was used to study the surface morphology of composite membranes and cellulose, at an acceleration voltage ranging within 0.02-30 kV. All the specimens were sputter coated with gold before imaging to enhance the conductivity and mitigate charging effects.

X-ray diffraction analysis

X-ray diffraction was carried out using a Malvern-Analytical X'pert3 powder diffractometer. Pistachio

shells were ground in a spice grinder (Model: NSG500B, Nilsan prime India Pvt. Ltd.). The powdered pistachio shells and extracted cellulose powder were scanned between 5 to 60° at a step size of 0.04°. The diffractometer was operated at a voltage of 40 kV and the current was 15 mA with CuK α radiation of wavelength 1.54 Å. The crystallinity index of the materials was calculated using Segal's equation based on the reflected intensity data:³⁴

$$\text{CrI (\%)} = \frac{I_{200} - I_{am}}{I_{200}} \times 100 \quad (4)$$

where I_{200} is maximum reflected intensity of the 002 lattice plane attributed to the crystalline part of cellulose, and I_{am} is minimum reflected intensity at $2\theta = 18^\circ$ attributed to the amorphous part of cellulose.

Mechanical properties

The tensile properties, encompassing tensile strength, elongation at break and Young's modulus of the EVA/cellulose composites were studied using a Universal Testing Machine (Instron 5965, USA), equipped with a 5 kN load cell. The tests were conducted in accordance with the ASTM D-882 standard, at a tensile speed of 50 mm/min.

RESULTS AND DISCUSSION

Structure and morphology of cellulose and EVA/cellulose composite membranes

Figure 1 shows the images of pistachio shell powder, alkali treated pistachio shell powder and cellulose prepared from pistachio shells. The creamy light beige coloured pistachio powder

changed to white coloured cellulose after alkali and bleaching treatments. Figures 2 and 3 show the SEM images under different magnifications of pistachio shells and isolated cellulose, respectively. It shows that the softer pistachio shell powder became rougher and possessed a network-like structure in isolated cellulose. It also reveals that cellulose isolated from the pistachio shell is irregular in shape. The length and width of cellulose fibers were calculated from SEM images using imageJ software. The average length of the cellulose fiber was 123.48 μm and the average width was 60.35 μm .

The cellulose was further characterized by FTIR and XRD. The FTIR spectra (see Fig. 4) show the successful removal of lignin and hemicelluloses from pistachio shell powder. Lignin contains several phenyl propane groups and its FTIR spectra show the peaks of -OH groups, aromatic rings, methylene and methyl group. Hemicelluloses contain several five-carbon and six-carbon sugars and uronic acids. Lignin, hemicelluloses and cellulose show FTIR peaks in the range 3000-3600 cm^{-1} , which indicates broad band stretching vibrations of OH groups, the frequency in the range 2800-2900 cm^{-1} comes from the stretching vibrations of C-H bonds in methylene and methyl groups.



Figure 1: Photographs of pistachio shell powder, alkali treated pistachio shell powder and isolated cellulose

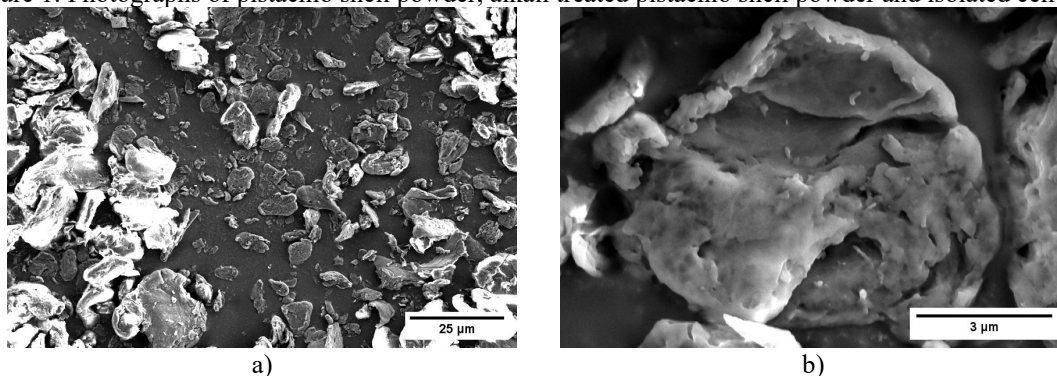


Figure 2: SEM images of pistachio shell powder under different magnifications (a and b)

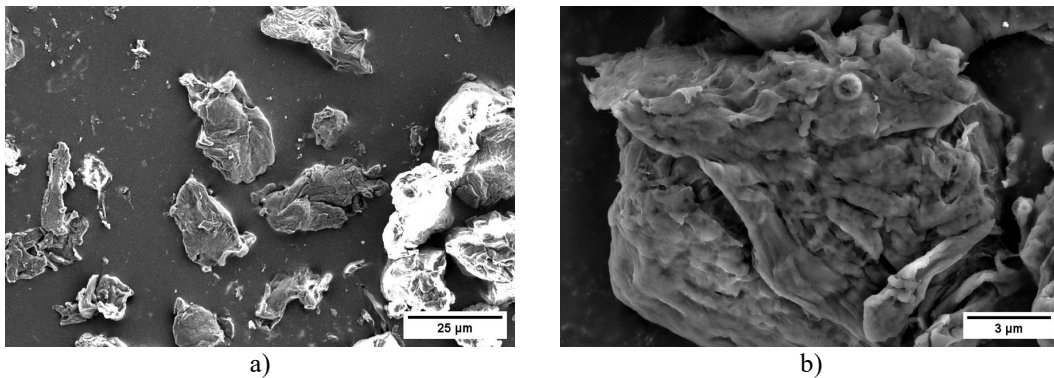


Figure 3: SEM images of cellulose under different magnifications (a and b)

The peak around 1500 cm^{-1} is attributed to the C=C stretching in the aromatic rings of lignin, the peak at 1734 cm^{-1} is assigned to the carbonyl, ester and acetyl groups of hemicelluloses and lignin, the frequency at 1241 cm^{-1} is caused by the C-O-C stretching of hemicelluloses and lignin. These three peaks are absent in the FTIR spectrum of cellulose, which shows the elimination of hemicelluloses and lignin. The frequencies at 1022 cm^{-1} and 897 cm^{-1} were ascribed to the C-O-C pyranose ring skeletal vibrations and the C-H rock vibrations in cellulose, respectively.

X-ray diffractograms (Fig. 5) show an improvement in the crystallinity index, as well as an increase in intensity of the crystalline peaks after the alkali and bleaching treatment. Pistachio shell powder has three diffraction peaks at $2\theta = 16, 22$ and 34.7° , which were assigned to the planes (1 1 0), (0 0 2) and (0 0 4), respectively.³⁵ The intensity of the crystalline peaks of cellulose at $2\theta = 16, 22$ and 34.7° was increased after alkali and bleaching treatments. The crystallinity index

of pistachio shell was 27% and that of the prepared cellulose was 58%, which was determined by the Segal method from the XRD spectra (Fig. 5). It also provides evidence for the elimination of the amorphous parts, such as lignin and hemicelluloses, from the pistachio shell powder.

Five types of EVA composite membranes were prepared by varying the weight of cellulose. FTIR spectra of the EVA pure polymer membrane and EVA/cellulose (10%) composite membrane are shown in Figure 6. The characteristic peaks of the vinyl acetate group in EVA can be seen at 1740 cm^{-1} , 1244 cm^{-1} , 1025 cm^{-1} and those of the ethylene groups of EVA are at 2925 cm^{-1} , 2849 cm^{-1} , 1462 cm^{-1} , 1367 cm^{-1} and 720 cm^{-1} . After the addition of cellulose to EVA, there is an increase in the intensity and width of the peaks around $3600\text{--}3000\text{ cm}^{-1}$ and 1025 cm^{-1} , which indicate the vibration of O-H groups and C-O-C pyranose ring skeletal vibration in cellulose, respectively. It clearly indicates the interaction of cellulose fibers with the polar groups of EVA.

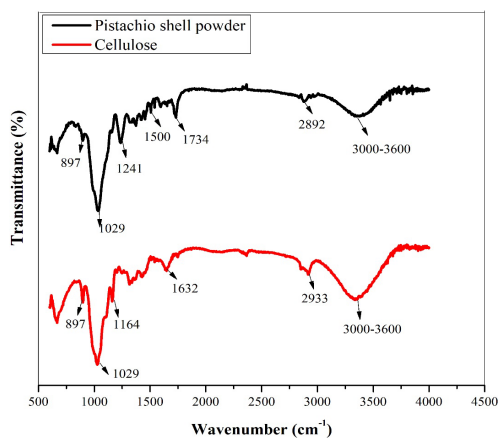


Figure 4: FTIR spectra of pistachio shell and cellulose fiber

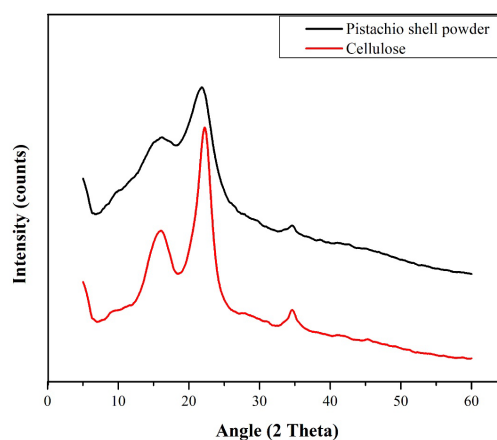


Figure 5: X-ray diffractograms of pistachio shell powder and cellulose from pistachio shell powder

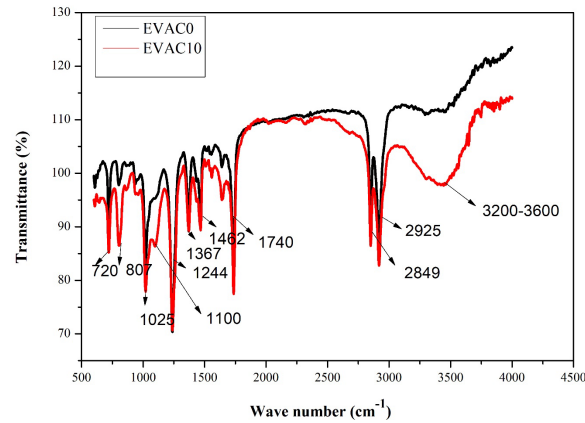


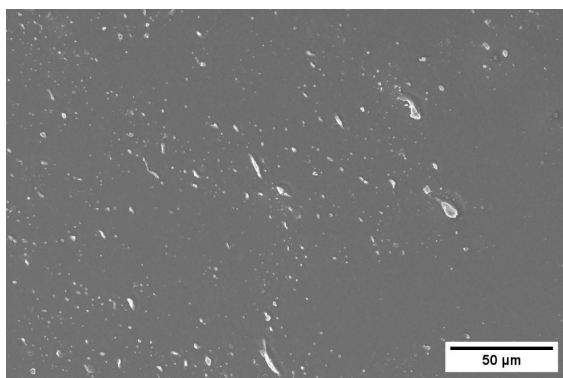
Figure 6: FTIR spectra of EVA and EVA/cellulose composite membranes

The morphology of EVA/cellulose composite membranes was studied using SEM images, which are shown in Figure 7. It describes the interaction and distribution of the cellulose filler in the EVA polymer. Figure 7a shows the scanning electron micrograph of the pure EVA polymer membrane, where the presence of pores is visible. Figure 7b shows the SEM micrograph of the EVA/cellulose 5% composite membrane, where particles are distributed in the polymer matrix in a good manner, without any considerable agglomeration.³⁶ The cellulose particles are agglomerated at a greater percentage of cellulose loading, as visible from the SEM micrograph of EVA/cellulose 10% composite membrane in Figure 7c.

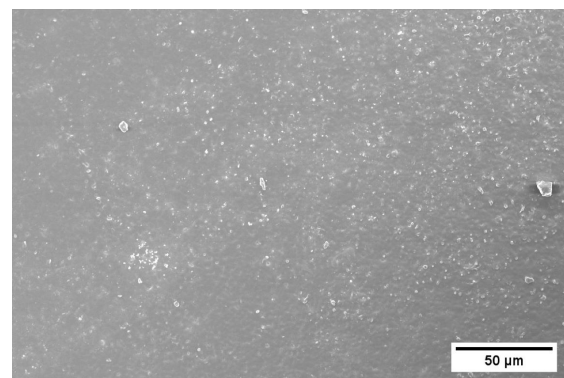
Mechanical properties of EVA/cellulose composite membranes

Figure 8 (a, b and c) shows the plots of tensile strength, elongation at break and Young's modulus of EVA/cellulose composite membranes at various cellulose loading. The EVA/cellulose composite membranes have lower tensile strength compared to the pure EVA membrane. The added

filler particles have micro-sized dimension (average length = 123.48 μm and average width = 60.35 μm), the low aspect ratio results in lower tensile strength of the composite membranes. The nanocrystalline cellulose or cellulose in nanodimension was proven to be the best filler to reinforce polymer membranes.³⁷ The shape of the filler also affects the tensile strength of the composite membranes. The loaded cellulose is irregular in shape and has low ability to support the stress transfer from the polymer matrix, and thus, the tensile strength decreases. Elongation at break also shows a decrease for cellulose loaded EVA composite membranes. It is a measure of deformation of a material before rupture or breaking. Here, the added cellulose filler makes the polymer composite stiffer and breaks the composite membrane more easily. The Young's modulus of the composite membranes shows a gradual increase with filler loading. It is the measure of the relative stiffness of the composites. The increase in the Young's modulus of the membranes is due to the stiffness of the cellulose fibers added.³⁸



a)



b)

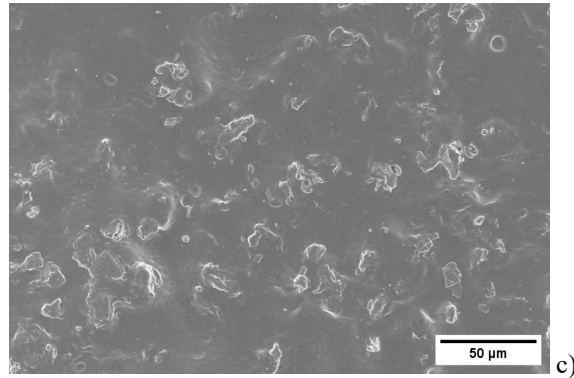


Figure 7: SEM micrographs of (a) EVA, (b) EVA/cellulose (5%) composite and (c) EVA/cellulose (10%) composite membranes

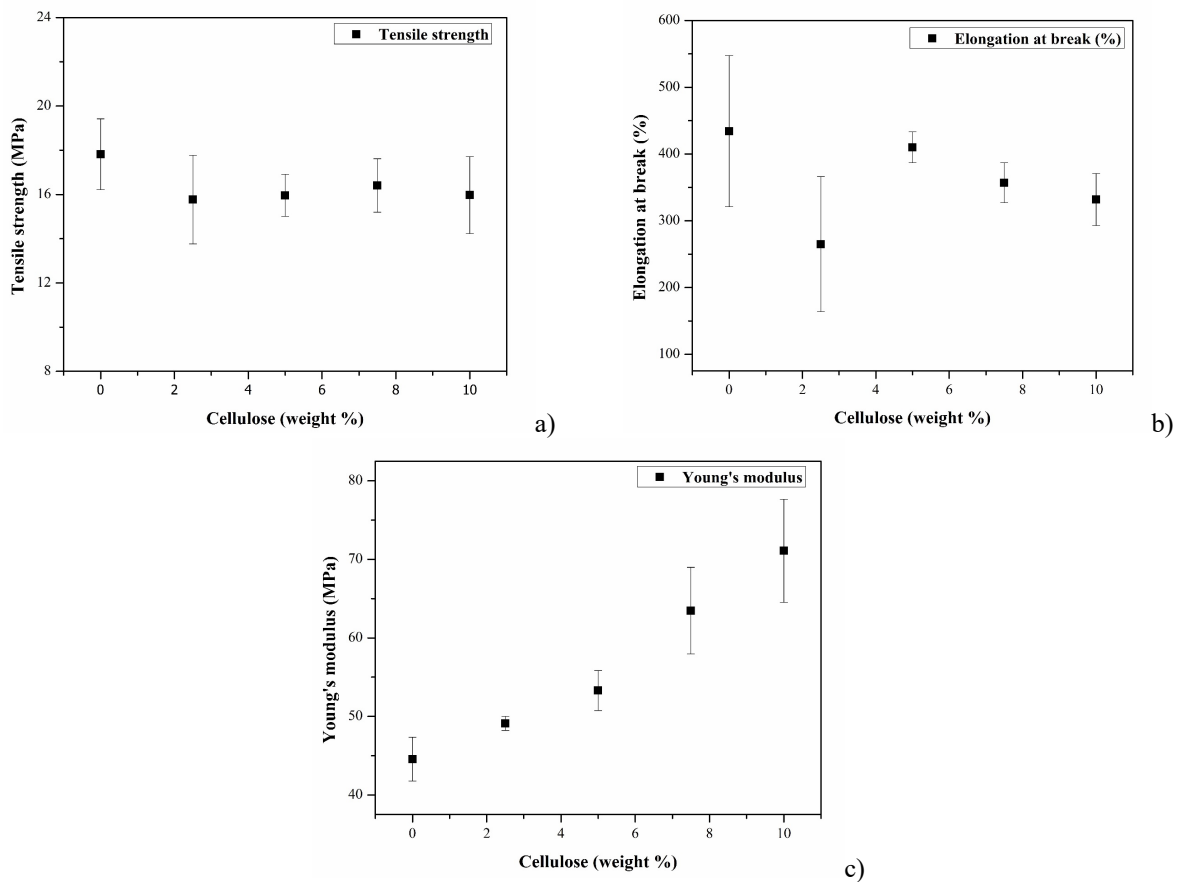


Figure 8: (a) Tensile strength, (b) elongation at break and (c) Young's modulus of composites

Vapour permeability measurements

The addition of cellulose fibers to the EVA polymer matrix introduces a tortuous pathway for the diffusing molecules. The permeation of two groups of organic solvents through the EVA/cellulose composite membranes was studied. The solvents from the first group were benzene, toluene and xylene (BTX solvents), which are non-polar solvents, and those from the second group were dichloromethane, chloroform and carbon tetrachloride (chlorosolvents), which

are polar solvents. At a given temperature, the evaporated solvent molecules undergo three processes: the vapour molecules first adsorb onto the polymer membrane, then they diffuse through the thickness of the membrane and finally get desorbed from the system. Here, the impermeable cellulose fibers increase the barrier property of the composite membranes, compared to the pure EVA membrane. This improvement can be attributed to two phenomena: a reduced diffusion area and lengthened diffusion time. The diffusion

area available for permeation of solvent molecules is decreased due to the occupation of the space within the permeable polymer matrix by impermeable cellulose fibers. Similarly, impermeable filler particles create a tortuous pathway in the matrix and the diffusing solvent molecules need to pass through these twists and turns, resulting in a prolonged diffusion time.

Permeation of non-polar solvents through the composite membranes

Figure 9 shows the permeation characteristics of EVA and EVA/cellulose composite membranes, where benzene is selected as the permeating solvent. It is evident from the plots that the permeation through the cellulose loaded EVA composite membrane is lower than through the pure EVA polymer membrane. A regular decrease in permeation is observed up to a filler loading of 5% in the composite membranes, followed by an increase in permeation above 5% loading of cellulose, but it is still lower than that of the pure EVA polymer membrane.

The lowering of permeation for the cellulose loading up to 5% is observed due to the uniform distribution of cellulose particles, while higher loading resulted in the agglomeration of filler particles. The porous nature of EVA can be seen in the SEM micrographs of the pure polymer membrane. These pores are filled by the incorporated cellulose fibers, creating a tortuous path for the solvent vapours. The polar -OH groups of cellulose have polar-polar interaction with the acetate groups in the EVA matrix, and good compatibility between EVA and cellulose creates a homogenous distribution of the cellulose filler up to an optimum loading. The vapour

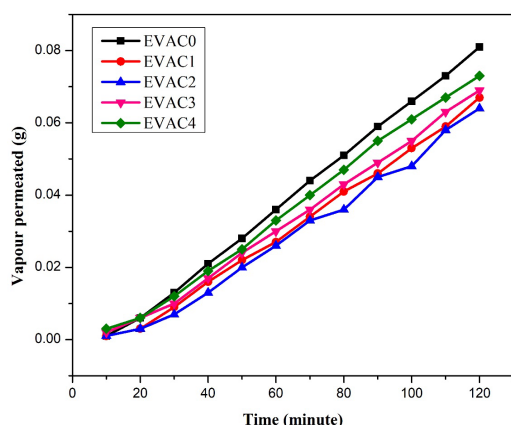


Figure 9: Permeation plots of composite membranes for benzene

molecule has to pass a longer distance in between the cellulose particles in the EVA/cellulose composite membranes. So, the permeation of the solvent through the composite membrane decreases. At higher loading of the filler, the cellulose-cellulose interaction dominates, and effective distribution of the filler in the polymer matrix becomes difficult, so the fibers start to agglomerate. So, the permeation of the solvent through the EVA/cellulose composite membranes increases beyond 5% loading of cellulose.

Figure 10 shows the permeation plots of benzene, toluene and xylene (non-polar solvents) through the EVAC2 composite membrane. The permeation of benzene vapours through the membrane is greater than the permeation of toluene and xylene vapours. This can be explained by the molar size and molecular mass of the penetrating solvents. The molar size and molecular mass of benzene are smaller than those of toluene and xylene, and so the vapour molecules with lower size will penetrate faster than large sized ones. Thus, the penetration of the studied solvents through the membrane was in the following order: benzene > toluene > xylene.

Permeation of polar solvents through the composite membranes

Permeation of chlorosolvents through the EVA/cellulose composite membrane gives similar results. The permeation plots of dichloromethane are shown in Figure 11. A regular lowering of permeation was observed up to 5% loading of cellulose in the EVA polymer, followed by an increase in permeation at higher loading. This is because uniform distribution of the filler is possible only up to 5% loading of cellulose.

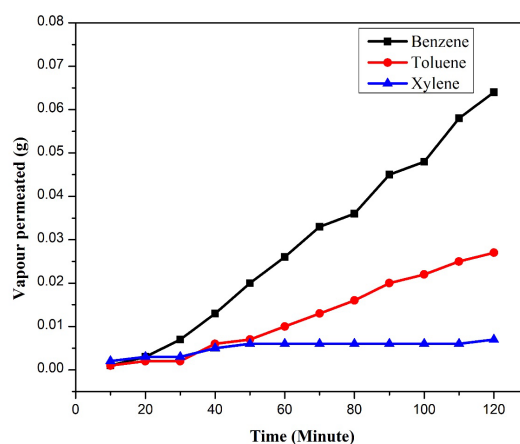


Figure 10: Comparison of vapour permeation of non-polar solvents through EVAC2

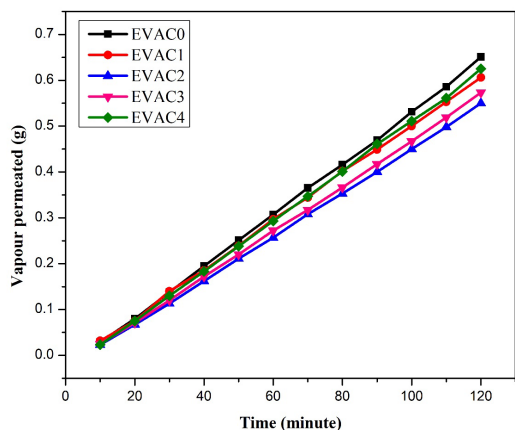


Figure 11: Permeation plots of composite membranes for dichloromethane

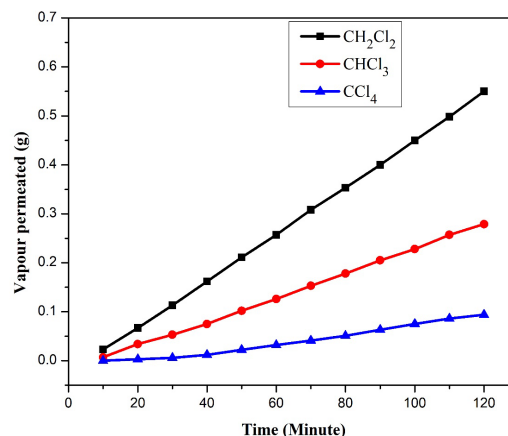


Figure 12: Comparison of vapour permeation of polar solvents through EVAC2

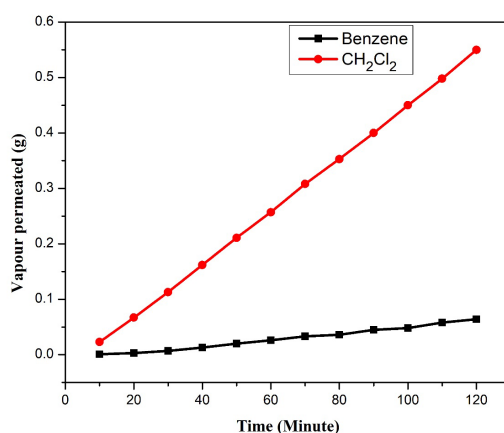


Figure 13: Permeation of benzene and dichloromethane through EVAC2

Agglomeration of cellulose particles occurs in the matrix with an increase in the weight of cellulose, which results in an increase in the permeation of polar solvents, as observed in the case of non-polar solvents.

Figure 12 shows the permeation plots of dichloromethane, chloroform and carbon tetrachloride (polar solvents) through the EVAC2 composite membrane. The permeation of dichloromethane vapours through the membrane is greater than the permeation of chloroform and carbon tetrachloride vapours. The permeation of different polar solvents through the membrane depends on the polarity, molar size and molecular mass of the penetrating solvents.³⁹ Thus, vapour permeation was found to be in the order: dichloromethane > chloroform > carbon tetra chloride.

Another finding regarding the permeation of two groups of solvents through the membranes is that the permeation values of polar solvents (chlorosolvents) are higher than that of the non-polar solvents (BTX solvents). Figure 13 compares the permeation of benzene and

dichloromethane through EVAC2, where the permeation of dichloromethane occurs to a higher extent than that of benzene. This is probably due to the polar nature of the EVA/cellulose composite membrane, which has higher affinity towards the polar chlorosolvents compared, to the BTX solvents.

Permeation coefficients

Studying the permeation coefficients of polymer membranes holds significant importance for assessing and optimizing their barrier properties. In material science and engineering, this tailored membrane design is vital in areas like packaging, where controlled permeability is essential. In the context of barrier properties, a lower permeation coefficient indicates a more effective barrier, as it suggests reduced permeability to certain substances. This is particularly important in industries, such as packaging for preserving the integrity, freshness and shelf life of products. Figures 14 and 15 give the permeation coefficients of BTX solvents and

chlorosolvents at different weight percentage of cellulose filler.

Examining the permeation coefficients of the EVA/cellulose composite membranes, a regular decrease can be observed for the membranes incorporating up to 5% cellulose loading, compared to the pure EVA polymer membrane, followed by an increasing tendency at higher loading of cellulose. For each penetrant, the permeation coefficient of the EVA/cellulose composites is less than that of the pure EVA polymer membrane. The decrease in permeation coefficient was due to the effective filling of pores in the EVA by cellulose particles. The increase in permeation coefficients beyond 5% loading of cellulose was attributed to the agglomeration of cellulose particles, which hindered the effective filling of pores in EVA. The permeation coefficients of the polymer membranes were also compared for polar and non-polar solvents, and the following order was found: benzene > toluene > xylene for non-polar solvents, and dichloromethane > chloroform > carbon tetrachloride for polar solvents. It indicates that the permeation coefficient depends on the molar size and molecular mass of penetrating solvents. It was also found that the permeation coefficients of composites for chlorosolvents are higher than those for BTX solvents. It is ascribed

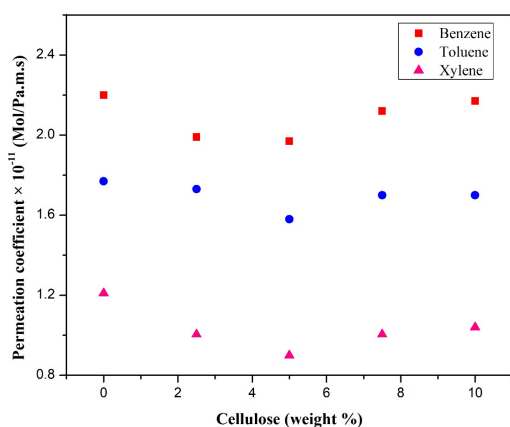


Figure 14: Permeation coefficients of composite membranes for non-polar solvents

This trend is seen up to 5% loading of cellulose due to uniform distribution of cellulose fiber in the EVA matrix, which is possible until this weight. For higher loading, cellulose-cellulose interactions lead to the aggregation of the filler in the matrix, there resulting higher permeability

to the fact that polar solvents are more attracted to the polar EVA/cellulose composite membranes.

Relative permeability

Examining the relative permeability of polymer membranes allows researchers to optimize their barrier properties. By tailoring the membrane's composition, structure or surface properties, they can enhance its ability to resist the permeation of unwanted substances. This knowledge is fundamental and contributes to advancements in areas, such as packaging, environmental protection, and the preservation of product quality and integrity. Tables 2 and 3 show the theoretical and experimental values of relative permeability of composites for chlorosolvents and BTX solvents. Figures 16 and 17 provide a comparison of theoretical and experimental values of relative permeabilities.

Theoretical relative permeability has a gradual decline in its values for parallel and random orientations of the filler. Experimental values of relative permeability decrease with cellulose loading up to 5% and then increase for both groups of solvents. The experimental and theoretical permeability values are nearly in the same range for lower loading of cellulose percentage.

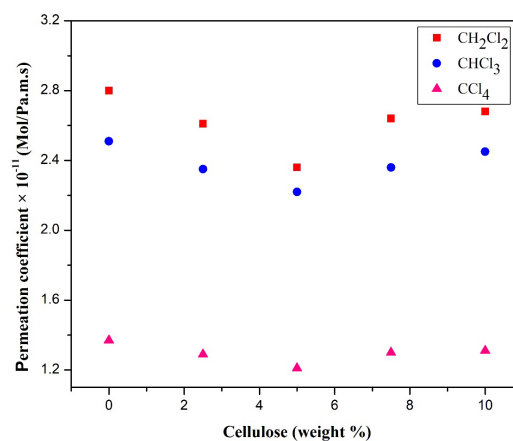


Figure 15: Permeation coefficients of composite membranes for polar solvents

values. The experimental value of relative permeability is in higher agreement with the theoretical value for S=1. So, we can conclude that the cellulose fibers have a parallel distribution in the EVA matrix.

Table 2
Experimental and theoretical values of relative permeability of composites for non-polar solvents

Samples	Experimental			Theoretical	
	Xylene	Toluene	Benzene	S = 1	S = 0
EVAC0	1	1	1	1	1
EVAC1	0.8305	0.9265	0.9045	0.9689	0.9792
EVAC2	0.7446	0.8926	0.8954	0.9396	0.9591
EVAC3	0.8305	0.9604	0.9636	0.9121	0.9462
EVAC4	0.8595	0.9604	0.9863	0.8861	0.9214

Table 3
Experimental and theoretical values of relative permeability of composites for polar solvents

Samples	Experimental			Theoretical	
	Xylene	Toluene	Benzene	S = 1	S = 0
EVAC0	1	1	1	1	1
EVAC1	0.8305	0.9265	0.9045	0.9689	0.9792
EVAC2	0.7446	0.8926	0.8954	0.9396	0.9591
EVAC3	0.8305	0.9604	0.9636	0.9121	0.9462
EVAC4	0.8595	0.9604	0.9863	0.8861	0.9214

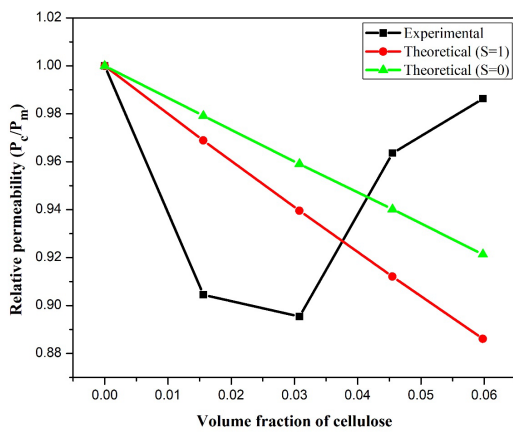


Figure 16: Relative permeability of composites with benzene as solvent

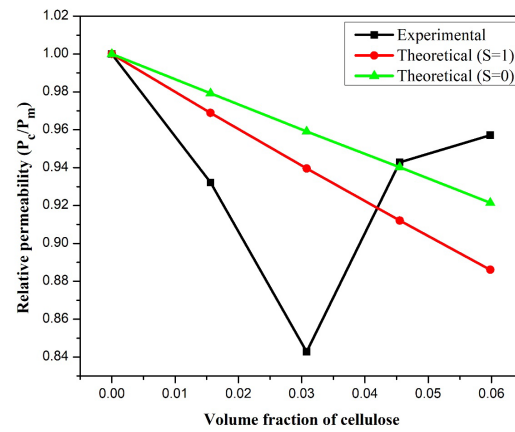


Figure 17: Relative permeability of composites with dichloromethane as solvent

Biodegradability of the composite membranes

The soil burial test was conducted under natural atmospheric conditions in a home garden situated in the Edavanna village of Malappuram district, Kerala, India. Visual examination of cellulose containing samples (see Fig. 18), which were taken out from the soil, revealed microbial colonies on the specimen. It indicates that the added cellulose fillers allow microbes to enter inside the EVA polymer, leading to biodegradation. Weight loss measurements and tensile strength analysis of the EVA/cellulose composites also revealed that the addition of cellulose to thermoplastic EVA is a good method to make the polymer composites partially degradable. After one month, 3.8% of weight loss and, after two months, 4.7% weight loss were

observed for the EVA/cellulose 5% composite membrane. When the percentage of the filler in the matrix was increased, an increased weight loss of the composites was observed. Namely, the EVA/cellulose 7.5% composite membrane had a higher weight loss – of about 6.8% after one month and of 7.8% after two months. The changes in weight loss of different membranes are shown in Figure 19. The pure EVA polymer membrane had no weight loss, which indicates that the microbes have no capacity to attack EVA plastic membrane, while the cellulose added to the EVA was consumed by microorganisms in the soil, which is the reason for the weight loss observed. If we increase the duration of the soil burial test, it will lead to the fragmentation of the EVA polymer and the formation of the low

molecular weight compounds by the action of microorganisms.

The tensile strength of the specimens was also evaluated before and after the soil burial and the percentage loss in tensile strength was calculated for two months. The tensile strength of a material is the key mechanical property that measures its ability to withstand stretching or pulling forces. By testing the polymer membranes after soil burial, it is possible to gain an insight into how well the materials maintain their structural

integrity and strength under the influence of soil-related environmental factors. So, this examination will help to evaluate the materials' performance under harsh real-world conditions and it is crucial for sustainable material development and effective waste management practices. Figure 20 shows the loss in tensile strength of the pure EVA membrane, EVA/cellulose 5% composite membrane and EVA/cellulose 7.5% composite membrane after the soil burial test.



Figure 18: EVA/cellulose 7.5% composite membranes before and after the soil burial test

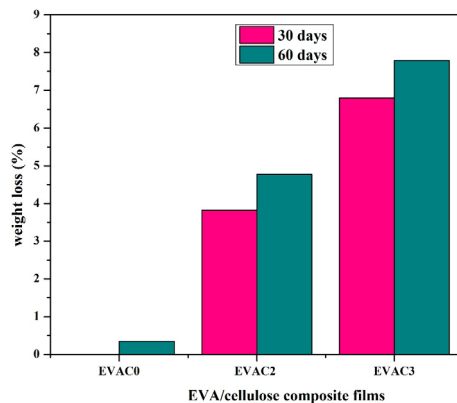


Figure 19: Percentage weight loss of pure EVA membrane and EVA/cellulose composite membranes

The tensile strength decreased in three types of membranes and the loss in tensile strength was higher for the cellulose filled composites. The decrease in tensile strength is attributed to the action of temperature, microorganisms and moisture of the soil, affecting the pure EVA membrane and the EVA/cellulose composite membranes differently. Specifically, the tensile strength decreased by approximately 30% for the EVA/cellulose 5% composite membrane and by around 24% for EVA/cellulose 7.5% composite membranes. The weight loss measurements and tensile strength analysis of composite membranes indicate the partial degradation of the EVA polymer composite membranes, transforming the

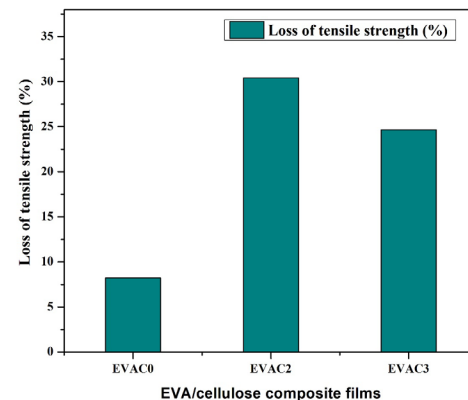


Figure 20: Loss of tensile strength of pure EVA and EVA/cellulose composite membranes after two months

non-biodegradable EVA into a material with reduced environmental impact.

CONCLUSION

Composite membranes were prepared with cellulose derived from pistachio shell and EVA at different loading of cellulose, and their structure, morphology, mechanical properties, vapour permeation properties and biodegradability were examined. FTIR and SEM analyses revealed the formation of composite membranes and uniform distribution of cellulose fibers up to 5% loading in the EVA matrix. Analysis of mechanical properties showed an increase in Young's modulus and a decrease in tensile strength and elongation at break. This trend can be explained

based on the ineffective stress transfer between EVA polymer and microsized cellulose fibers. Organic vapour permeability of the composite membranes gradually decreased with the increase in cellulose loading up to 5%, due to an increasingly tortuous path created by the filler impeding the diffusion of the penetrant. The increase in permeability at higher loading was caused by the agglomeration of cellulose, as evident from the SEM analysis. The permeation coefficients and relative permeability values of composites for chlorosolvents and BTX solvents were also calculated and they followed the same trend. Chlorosolvents were found to be more easily penetrating than BTX solvents owing to the polarity of EVA/cellulose composite membranes. The experimental values of relative permeability were discovered to be in good agreement with the theoretical values calculated using Baradwaj's permeability model, especially at lower loading of cellulose. It can be concluded that microcellulose fibers can improve the barrier performance of the EVA polymer. A decrease in tensile strength of the EVA polymer will be a disadvantage, but it can be improved by producing cellulose nanofibers from microcellulose. Cellulose fibers incorporated in the EVA polymer made the EVA/cellulose polymer composite membranes partially biodegradable, and thus, such fibers are good candidates for producing eco-friendly packaging materials.

ACKNOWLEDGEMENTS: The authors acknowledge the funding support from the Junior Research Fellowship of University Grants Commission, Ministry of Human Resource and Development, India (UGC reference No.: 58/(CSIR-UGC NET JUNE 2017).

REFERENCES

- M. H. Jawaid and H. A. Khalil, *Carbohydr. Polym.*, **86**, 1 (2011), <https://doi.org/10.1016/j.carbpol.2011.04.043>
- V. K. Thakur and M. K. Thakur, *Carbohydr. Polym.*, **109**, 102 (2014), <https://doi.org/10.1016/j.carbpol.2014.03.039>
- P. Cazón and M. Vázquez, *Environ. Chem. Lett.*, **18**, 257 (2020), <https://doi.org/10.1007/s10311-019-00936-3>
- H. M. De Azeredo, *Food. Res. Int.*, **42**, 1240 (2009), <https://doi.org/10.1016/j.foodres.2009.03.019>
- S. Elanthikkal, T. Francis, G. Unnikrishnan, S. Varghese and J. T. Guthrie, *Polym. Eng. Sci.*, **52**, 2140 (2012), <https://doi.org/10.1002/pen.23172>
- C. Wolf, H. Angellier-Coussy, N. Gontard, F. Doghieri and V. Guillard, *J. Membr. Sci.*, **556**, 393 (2018), <https://doi.org/10.1016/j.memsci.2018.03.085>
- R. K. Bharadwaj, A. R. Mehrabi, C. Hamilton, C. Trujillo, M. Murga *et al.*, *Polymer*, **43**, 3699 (2002), [https://doi.org/10.1016/S0032-3861\(02\)00187-8](https://doi.org/10.1016/S0032-3861(02)00187-8)
- K. G. Gatos and J. Karger-Kocsis, *Eur. Polym. J.*, **43**, 1097 (2007), <https://doi.org/10.1016/j.eurpolymj.2007.01.032>
- J. K. Fink, "Handbook of Engineering and Specialty Thermoplastics", Vol. 1: Polyolefins and Styrenics, John Wiley & Sons, 2010
- M. Sadeghi, G. Khanbabaei, A. H. S. Dehaghani, M. Sadeghi, M. A. Aravand *et al.*, *J. Membr. Sci.*, **322**, 423 (2008), <https://doi.org/10.1016/j.memsci.2008.05.077>
- M. Shafiee and S. A. A. Ramazani, *Macromol. Symp.*, **274**, 1 (2008), <https://doi.org/10.1002/masy.200851401>
- M. A. Zamiri, A. Kargari and H. Sanaeepur, *Greenh. Gas. Sci. Technol.*, **5**, 668 (2015), <https://doi.org/10.1002/ghg.1513>
- R. Wilson, T. S. Plivelic, A. S. Aprem, C. Ranganathaiah, S. A. Kumar *et al.*, *J. Appl. Polym. Sci.*, **123**, 3806 (2012), <https://doi.org/10.1002/app.34966>
- T. P. Selvin, J. Seno, B. Murukan, A. A. Santhosh, T. Sabu *et al.*, *Polym. Compos.*, **31**, 1011 (2010), <https://doi.org/10.1002/pc.20887>
- M. A. Hubbe, A. Ferrer, P. Tyagi, Y. Yin, C. Salas *et al.*, *BioResources*, **12**, 2143 (2017)
- S. H. Othman, N. A. Majid, I. S. Tawakkal, R. K. Basha, N. Nordin *et al.*, *Food. Sci. Technol.*, **39**, 605 (2019), <https://doi.org/10.1590/fst.36017>
- P. Dhar, S. S. Gaur, N. Soundararajan, A. Gupta, S. M. Bhasney *et al.*, *Ind. Eng. Chem. Res.*, **56**, 4718 (2017), <https://doi.org/10.1021/acs.iecr.6b04699>
- H. Adelnia, H. C. Bidsorkhi, A. F. Ismail and T. Matsuura, *Sep. Purif. Technol.*, **146**, 351 (2015), <https://doi.org/10.1016/j.seppur.2015.03.060>
- M. Amini, S. A. Haddadi and A. Kheradmand, *Diam. Relat. Mater.*, **99**, 107523 (2019), <https://doi.org/10.1016/j.diamond.2019.107523>
- S. Eskandarabadi, M. Mahmoudian, M. Farah, K. R. Abdali, A. Nozad *et al.*, *Food Packag. Shelf Life*, **22**, 100389 (2019), <https://doi.org/10.1016/j.fpsl.2019.100389>
- T. T. de Barros-Alexandrino, M. M. Tosi and O. B. G. Assis, *Polym. Eng. Sci.*, **59**, E287 (2019), <https://doi.org/10.1002/pen.24938>
- J. Wang, D. J. Gardner, N. M. Stark, D. W. Bousfield, M. Tajvidi *et al.*, *ACS Sustain. Chem. Eng.*, **6**, 49 (2018), <https://doi.org/10.1021/acssuschemeng.7b03523>
- R. A. Chowdhury, M. Nuruddin, C. Clarkson, F. Montes, J. Howarter *et al.*, *ACS Appl. Mater. Interfaces*, **11**, 1376 (2018), <https://doi.org/10.1021/acsami.8b16897>

- ²⁴ I. Paterniti, D. Impellizzeri, M. Cordaro, R. Siracusa, C. Bisignano *et al.*, *Nutrients*, **9**, 915 (2017), <https://doi.org/10.3390/nu9080915>
- ²⁵ S. A. Hassan, M. Abbas, S. Zia, A. A. Maan, M. K. I. Khan *et al.*, *Crit. Rev. Food Sci. Nutr.*, (2022), <https://doi.org/10.1080/10408398.2022.2130158>
- ²⁶ M. Ahanchi, M. Tabatabaei, M. Aghbashlo, K. Rezaei, A. F. Talebi *et al.*, *J. Clean. Prod.*, **185**, 852 (2018), <https://doi.org/10.1016/j.jclepro.2018.03.089>
- ²⁷ C. A. Igwegbe, J. O. Ighalo, S. Ghosh, S. Ahmadi and V. I. Ugonabo, *Biomass. Convers. Biorefin.*, **13**, 8793 (2023), <https://doi.org/10.1007/s13399-021-01739-9>
- ²⁸ S. Y. Nayak, S. S. Heckadka, U. A. Kini, L. G. Thomas and I. Gupta, in *Procs. International Conference on Engineering and Information Technology*, Kuala Lumpur, Malaysia, March 17-18, 2017, pp. 17-24
- ²⁹ B. Karaağaç, *Polym. Compos.*, **35**, 245 (2014), <https://doi.org/10.1002/pc.22656>
- ³⁰ A. Thiagarajan, K. Velmurugan and P. P. Sangeeth, *Mater. Today: Proc.*, **39**, 610 (2021), <https://doi.org/10.1016/j.matpr.2020.09.001>
- ³¹ A. Mahmoodi, S. Ghodrati and M. Khorasani, *ACS Omega*, **4**, 14947 (2019), <https://doi.org/10.1021/acsomega.9b01731>
- ³² R. K. Bharadwaj, *Macromolecules*, **34**, 9189 (2001), <https://doi.org/10.1021/ma010780b>
- ³³ S. Y. Yap, S. Sreekantan, M. Hassan, K. Sudesh and M. T. Ong, *Polymers*, **13**, 104 (2020), <https://doi.org/10.3390/polym13010104>
- ³⁴ L. G. Segal, J. J. Creely, A. E. Martin Jr. and C. M. Conrad, *Text. Res. J.*, **29**, 786 (1959), <https://doi.org/10.1177/004051755902901003>
- ³⁵ N. Kasiri and M. Fathi, *Int. J. Biol. Macromol.*, **106**, 1023 (2018), <https://doi.org/10.1016/j.ijbiomac.2017.08.112>
- ³⁶ S. A. Paralikar, J. Simonsen and J. Lombardi, *J. Membr. Sci.*, **320**, 248 (2008), <https://doi.org/10.1016/j.memsci.2008.04.009>
- ³⁷ S. Elanthikkal, U. Gopalakrishnanpanicker, S. Varghese, J. T. Guthrie and T. Francis, *Carbohydr. Polym.*, **95**, 773 (2013), <https://doi.org/10.1016/j.carbpol.2013.02.039>
- ³⁸ C. Annandarajah, A. Langhorst, A. Kiziltas, D. Grewell, D. Mielewski *et al.*, *Materials*, **12**, 3189 (2019), <https://doi.org/10.3390/ma12193189>
- ³⁹ P. V. Anil Kumar, S. A. Kumar, K. T. Varughese and S. Thomas, *Sep. Sci. Technol.*, **47**, 811 (2012), <https://doi.org/10.1080/01496395.2011.630053>